arXiv:1304.6520v1 [astro-ph.GA] 24 Apr 2013

THE MYSTERIOUS SICKLE OBJECT IN THE CARINA NEBULA:
A STELLAR WIND INDUCED BOW SHOCK GRAZING A CLUMP?

Judith Ngoumou[1], Thomas Preibisch[1], Thorsten Ratzka[1], Andreas Burkert [1]
Universitäts-Sternwarte München, Ludwig-Maximilians-Universität, Scheinerstr.1, 81679 München, Germany
Draft version April 25, 2013

ABSTRACT

Optical and near-infrared images of the Carina Nebula show a peculiar arc-shaped feature, which we call the "Sickle", next to the B-type star *Trumpler 14 MJ 218*. We use multi-wavelength observations to explore and constrain the nature and origin of the nebulosity. Using sub-mm data from APEX/LABOCA as well as *Herschel* far-infrared maps, we discovered a dense, compact clump with a mass of $\sim 40 \, M_\odot$ located close to the apex of the Sickle. We investigate how the B-star MJ 218, the Sickle, and the clump are related. Our numerical simulations show that, in principle, a B-type star located near the edge of a clump can produce a crescent-shaped wind shock front, similar to the observed morphology. However, the observed proper motion of MJ 218 suggest that the star moves with high velocity ($\sim 100 \, \mathrm{km \, s^{-1}}$) through the ambient interstellar gas. We argue that the star is just about to graze along the surface of the clump, and the Sickle is a bow shock induced by the stellar wind, as the object moves supersonically through the density gradient in the envelope of the clump.

Subject headings: infrared: ISM — submillimeter: ISM — shock waves — stars: winds, outflows — stars: individual(Trumpler 14 MJ 218) — X-rays: stars

1. INTRODUCTION

The Carina Nebula is a complex star forming region situated at a distance of 2.3 kpc from the sun. With more than 70 massive stars identified (Smith & Brooks 2007), it is an ideal site to study the impact of stellar feedback on the interstellar medium (ISM). In this highly dynamical environment massive stars affect the surrounding medium through photoionizing radiation, stellar winds and ultimately through supernova explosions. Observations and numerical simulations have shown that these mechanisms can produce various observable morphologies like superbubbles at large scales (Oey & García-Segura 2004; Ntormousi et al. 2011), cavities (Fierlinger et al. 2012), shells (Deharveng et al. 2010; Walch et al. 2012) or pillars (Gritschneder et al. 2010; Preibisch et al. 2011a; Walch et al. 2012). The feedback mechanisms at work during the lifetime of the massive stars (before the supernova) may not play the most dominant role on larger scales (Dale & Bonnell 2011). However, these processes can affect the star formation locally by either triggering the formation of new stars (Gritschneder et al. 2010; Walch et al. 2012; Ohlendorf et al. 2012) or dispersing clouds and thereby delaying or even hindering star formation (Walch et al. 2012).

In addition to the feedback mechanisms mentioned above, the dynamical evolution of these massive stars is also likely to affect the surroundings. While most of the massive stars are believed to lie within their native OB association (Lada & Lada 2003) and are likely to be part of a binary or multiple system (Kobulnicky & Fryer 2007; Preibisch et al. 2001; Mason et al. 1998), some stars with quite high velocities, so called runaways, have been observed outside of OB associations (Blaauw 1961; Kobulnicky et al. 2012; Gvaramadze et al. 2012).

In this article we take a look at multi-wavelength observations of a peculiar nebulosity around a star in the Carina Nebula and the identification of a denser molecular clump at the same location. We interpret the crescent-shaped nebulosity, which we call the 'Sickle', as the tip of a bow shock associated with the B1.5 V star *Trumpler 14 MJ 218* (MJ 218 hereafter) listed in Massey & Johnson (1993). We discuss a possible link between the star, the Sickle and the clump and argue that the star is moving supersonically through the ambient density gradient on the front side of the observed compact clump.

The object caught our attention because of its peculiar morphology in our inspection of optical images of the Carina Nebula region. It is located about $1'$ south-east of the dense young cluster Tr 14, which corresponds to a projected physical distance of about 0.8 pc.

A literature search showed that the peculiar nebulosity had already been mentioned in the near-infrared (NIR) imaging study of the Tr 14 region by Ascenso et al. (2007), who suggested the idea of a compact HII region around the star. The highly asymmetric shape of the nebula could be the result of the irradiation from the very luminous early O-type stars in the center of Tr 14 (most notably the O2If star HD 93129A), since the apex of the crescent points toward this direction. Smith et al. (2010), however, noted that the lack of detectable Hα emission is in conflict with the interpretation as an HII region; they rather argued that the crescent nebula is a dusty bow shock.

Our investigation of the comprehensive multi-wavelength data set of the Carina Nebula that we compiled during the last years shows that the crescent nebula also appears to be related to a compact clump, which is (naturally) invisible in the optical and NIR images, but quite prominent in our far-infrared and sub-mm data. This makes the nebula even more interesting.

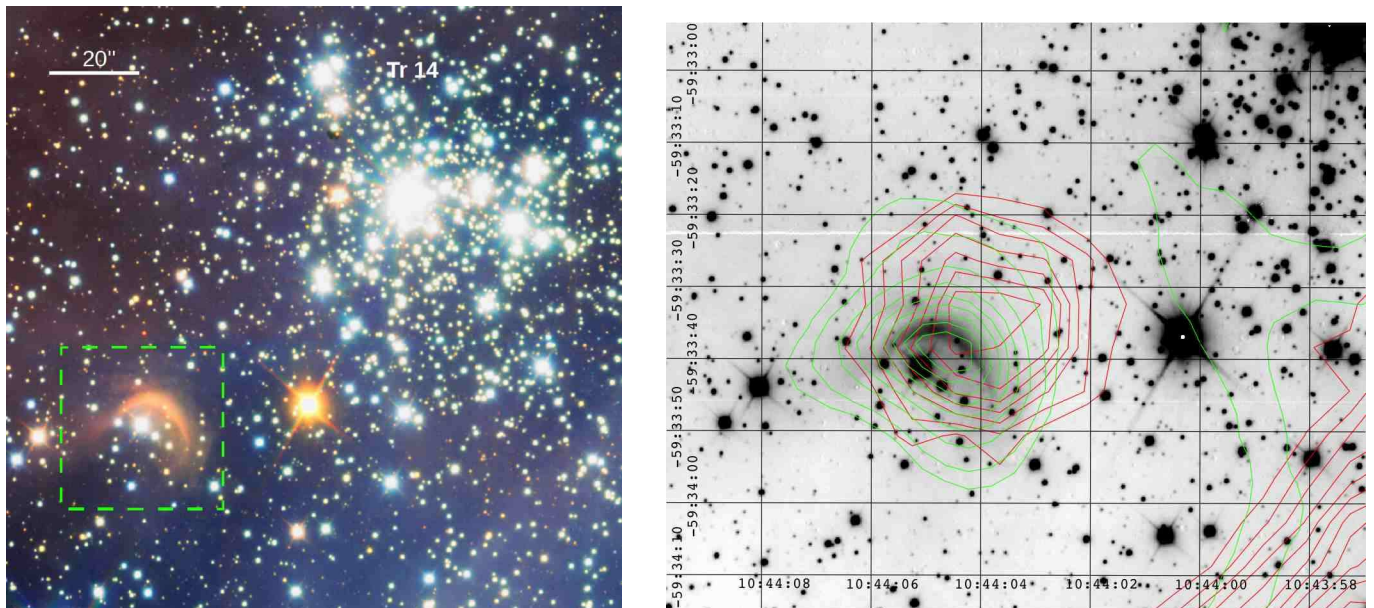ngoumou@usm.lmu.de

2. OBSERVATIONAL DATA AND RESULTS

FIG. 1.— left: RGB composite image constructed from the J- (blue), H- (green), and K_s-band (red) HAWK-I images of the area around the Sickle object (marked by the green dashed box in the lower left part) and the cluster Tr 14 (see also ESO photo release 1208; http://www.eso.org/public/news/eso1208/).
right: Negative grayscale representation of the K_s-band HAWK-I image of the area around the Sickle object with superposed contours of our *Herschel* 70 μm map (green) and our APEX/LABOCA 870 μm map (red). The contours levels of *Herschel* 70 μm map are at 2.25, 2.5, 3.0, 3.5, 4.0, 4.5, 5.5, and 6.0 Jy/pixel (pixel size 3.2″); the rms noise level in the map is $\sim$ 2.3 Jy/pixel. The contour levels of the APEX/LABOCA 870 μm map go from 0.05 Jy/beam to 0.5 Jy/beam in steps of 0.05 Jy/beam; as the rms noise level in the map is $\sim$ 0.02 Jy/beam, the first contour corresponds to the $\sim$ 2.5 σ level. Note that the horizontal bright streak in the background image is an artifact related to the dither pattern and the mosaicing process.

Stellar parameters — The observed crescent is associated to the B1.5 V star MJ 218 as listed by Massey & Johnson (1993) in their spectroscopic and photometric analysis of the stars in and around the clusters Trumpler 14 and Trumpler 16. MJ 218 alias *2MASS J10440508-5933412*, alias *ALS 19740* in Reed (2003) is located at the J2000 coordinates $10^h 44^m 05.1^s$, $-59° 33' 41''$, at about $1'$ south-east from the center of Tr 14. With optical/NIR magnitudes of $V = 11.85$ and $K = 9.63$ the star is a bright and prominent object. The stellar spectral type was determined via optical spectroscopy by Massey & Johnson (1993). These properties are very well consistent with the assumption that this star is a member of the Carina Nebula at a distance of 2.3 kpc.

In the UCAC4 Catalogue (Zacharias et al. 2012, 2013)[1], the star is listed as UCAC4 153-055048. Its proper motion is given as pm(RA) $= -7.0 \pm 3.0$ mas yr^{-1} and pm(Dec) $= 5.2 \pm 3.7$ mas yr^{-1}. The total proper motion of 8.7 ± 4.8 mas yr^{-1} corresponds to 95 ± 52 km s^{-1}. This is a remarkably high velocity, but we have to note that the uncertainties are quite large. Using the radial velocity of $v_{\rm rad} = -10.9$ km s^{-1} (Huang & Gies 2006) leads to a total space velocity of $v_* \approx 96$ km s^{-1}. This large velocity suggest that MJ 218 is a runaway star.

We note that the amplitude and direction of the motion would be consistent with the idea that the star MJ 218 could have been ejected some 66 000 years ago from the region of the open cluster Tr 16 which is at a distance of ~ 6.5 pc.

TABLE 1
JOURNAL OF HST OBSERVATIONS.

Filter	Date	Exp. Time[s]	Proposal IDs
F435W	2006-07-29	698	10602 (PI: J.Maiz Appellaniz)
F502N	2010-02-01	7650	12050 (PI: Mario Livio)
F550M	2006-07-29	678	10602 (PI: J.Maiz Appellaniz)
F658N	2005-07-17	1000	10241 (PI: Nathan Smith)
F775W	2003-05-17	550	9575 (PI: William B. Sparks)
F850LP	2006-07-29	678	10602 (PI: J.Maiz Appellaniz)

Hubble Space Telescope optical images — We searched the *Hubble* Legacy Archive for observations of the Sickle object. The images shown in Fig. 2 are taken with the Advanced Camera for Surveys (ACS). The dates of the observations, the exposure times, and the proposal identifiers are given in Table 1. Fig. 2 shows the compilation of HST in different filters, which reveal the small-scale structure of the nebulosity in detail. Two additional shells are visible closer to the star. Whereas the nebulosity is very well visible in the broad-band filters, neither the F502N band filter (tracing the [O III] line) nor the F658N filter (tracing the Hα line) reveal significant diffuse emission, clearly showing that the emission from the crescent nebula is not line-emission but continuum emission.

Near-infrared images — To investigate the near-infrared morphology of the nebula, we inspected data obtained in January 2008 as part of our survey of the Carina Nebula (see Preibisch et al. 2011d, for more details) with the instrument HAWK-I at the ESO 8m Very Large Telescope. Images were obtained in the standard J-, H-, and K_s-band filters, as well as in narrow-band filters centered on the 2.121 μm $\nu = 1 - 0$ S(1) ro-vibrational emission
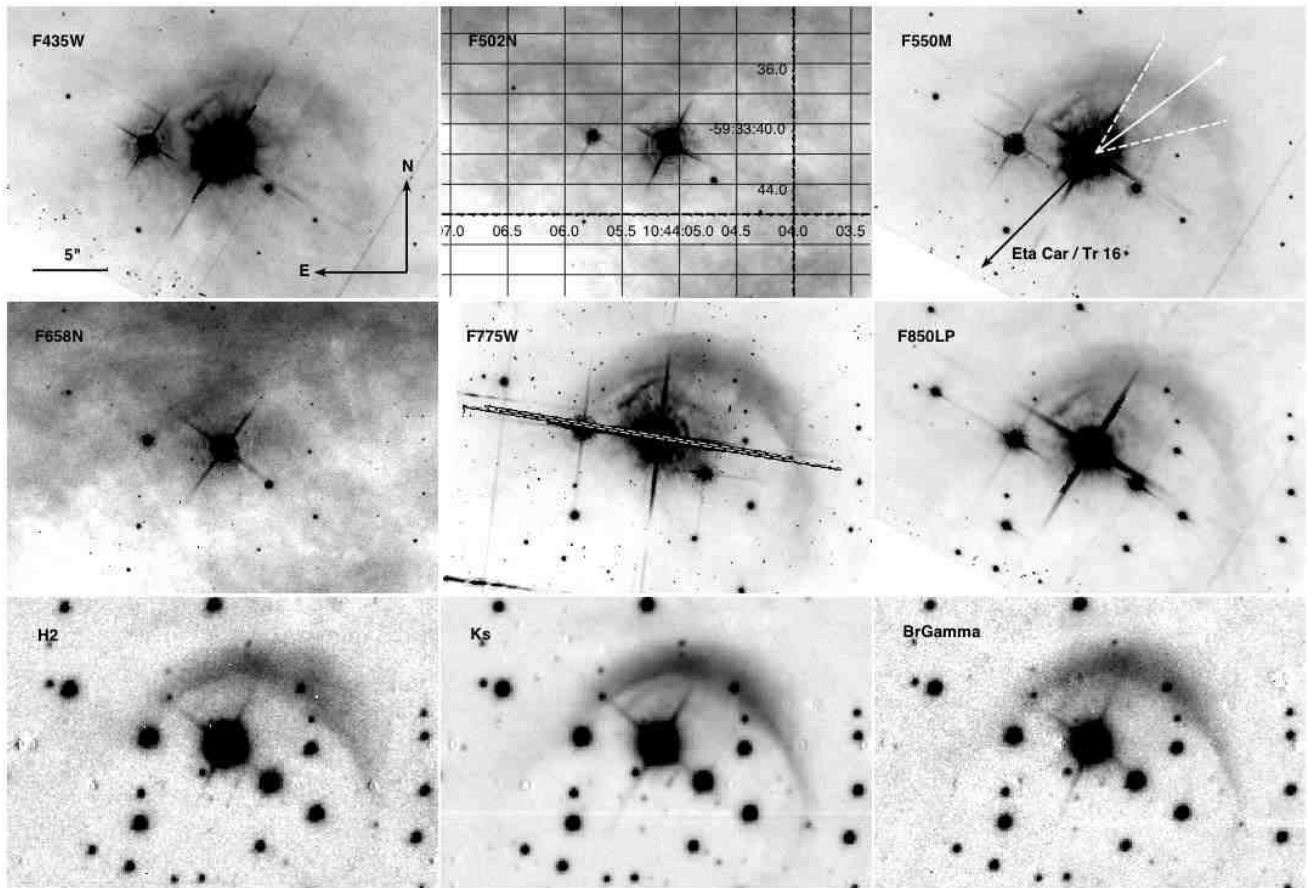
FIG. 2.— Images of the object taken with the HST (top and middle) and HAWK-I (bottom). A linear scale is used. The direction of the catalogued proper motion is indicated as a white arrow in the third panel (upper right). The uncertainty in the position angle of the velocity vector is indicated by the white dashed lines. The black arrow denotes the direction to η Carinae in Tr 16. In the fifth panel the prominent double diffraction spike is marked, indicating a bright compact source close to the B1.5V star..

line of molecular hydrogen and the 2.166 μm Bracket γ line. The very good seeing conditions during these observations resulted in sub-arcsecond FWHM values of typically 0.37″ (in the K_s-band) for the PSF size of point-like sources near the Sickle object.

Comparison of the narrow-band images with the K_s-band image shows: In the Bracket γ line, there is no increase of the brightness of the nebula relative to the star MJ 218. This excludes significant hydrogen line emission. Furthermore, there is also no indication of Bracket γ rim-brightening at the northern edge of the Sickle. Such a rim-brightening is clearly visible in narrow-band images in many of the irradiated globules in the Carina Nebula as well as in optical and near infrared images of photoevaporating globules and pillars (Smith et al. 2003, 2004). Rim-brightening highlights the strong surface irradiation by the surrounding hot stars. For the Sickle nebula, however, external irradiation seems not to be important.

In the molecular hydrogen line narrow-band image the relative brightness of the Sickle nebula is not much larger than in the broad-band image, but the nebulosity seems to be slightly more extended at the north-western edge. This suggests moderate amounts of molecular hydrogen line emission at the front of the nebula, similar as often observed in the bow-shocks of protostellar jets that move through molecular clouds (Preibisch et al. 2011d;

Tapia et al. 2011).

Mid-Infrared data: MSX and TIMMI2— The Sickle nebula coincides with the Midcourse Space Experiment (MSX) point source MSX6C G287.4288-00.5804. Mottram et al. (2007) performed mid-infrared imaging of this source with better angular resolution at the 3.6 m ESO Telescope and resolved the MSX source into four MIR sources. Their 10.4 μm image clearly shows the Sickle nebula (but no sign of the star MJ 218), and the peak of the emission corresponds very well to the brightest point of the Sickle as seen in our K_s-band image. Urquhart et al. (2007) and Mottram et al. (2007) reported a non-detection in radio continuum emission from this source. Urquhart et al. (2007) stated a detection limit of 0.4 mJy. Assuming an electron temperature of 10^4 K and the distance of 2.3 kpc, we derived an excitation parameter of $\sim 2\,\mathrm{pc\,cm^{-2}}$. By extrapolating Table 14.1 in Wilson et al. (2009), this value appears roughly consistent with a B1.5 star.

LABOCA sub-mm map— Whereas the optical and NIR images show no indication for the presence of a dense clump in the surroundings of the Sickle nebula, our 870 μm map that was obtained in December 2007 with the bolometer array LABOCA at the APEX telescope (see Preibisch et al. 2011a, for a complete description of

this data set) clearly reveals a compact clump located close to the tip of the Sickle. The position of the peak of the sub-mm emission is $10^h 44^m 04.06^s$, $-59° 33' 35.5''$, i.e. 10 arcseconds (or 0.1 pc) north-west of the star MJ 218 and about 3 arcseconds north-west of the apex point of the Sickle nebula. The sub-mm emission is almost point-like and only marginally extended; given the $18''$ angular resolution of LABOCA, the width of the clump is ~ 0.2 pc. The peak of the clump emission has an intensity of 0.393 Jy/beam.

Herschel far-infrared maps— Maps of the Carina Nebula at the wavelengths of 70, 160, 250, 350, and 500 μm were obtained in December 2010 in the Open Time project OT1-tpreibis-1 using the parallel fast scan mode at $60''$/s for simultaneous imaging with PACS (Poglitsch et al. 2010) and SPIRE (Griffin et al. 2010). A full description of these observations and the subsequent data processing can be found in Preibisch et al. (2012). The angular resolution of the *Herschel* maps is $5''$, $12''$, $18''$, $25''$, and $36''$ for the 70, 160, 250, 350, and 500 μm band, respectively. At a distance of 2.3 kpc this corresponds to physical scales ranging from 0.06 to 0.4 pc.

The clump near the Sickle nebula detected by LABOCA is clearly visible in the *Herschel* maps. It is clearly extended in the PACS maps, where we determine FWHM values of $19'' \times 16''$. These maps also show that the shape of the clump is not central symmetric. It exhibits a kidney-shaped form (green contours in Fig. 1, right panel), with a slight caved-in side in south-east direction in accordance with the inner side of the Sickle nebula bow. This clearly suggests that the process creating the Sickle nebula bow interacts with the clump.

Using the methods described in Preibisch et al. (2012), we determined the column density, temperature, and mass of the clump. The peak value for the column density in the center of the clump is $N_H \approx 1.3 \times 10^{22}$ cm^{-2}, corresponding to a visual extinction of $A_V \approx 6.5$ mag assuming a normal extinction law (note that these numbers are beam-averaged values, i.e. the true values for a line-of-sight exactly through the center will be higher). The dust temperature in the clump is found to be about 32 K. The mass of the clump can be determined by integrating the column density over all pixels exceeding the limit $A_V > 3$ mag (in order to separate the clump from the surrounding diffuse gas); this yields $M_{clump} \approx 40\,M_\odot$.

X-ray data— The object is located in the area covered by the *Chandra* Carina Complex Project, that recently mapped a 1.3 square-degree region of the Carina Nebula. With an exposure time of ~ 60 ksec (~ 17 hours) for the individual mosaic positions, the on-axis completeness limit is $L_X \approx 10^{29.9}$ erg/s in the $0.5 - 8$ keV band for lightly absorbed sources. A complete overview of the *Chandra* Carina Complex Project can be found in Townsley et al. (2011), which is the introduction to a set of 16 papers resulting from this project.

In the *Chandra* images analyzed in the context of the CCCP, the star MJ 218 is clearly detected as an X-ray point-source with 59 source counts. The J2000 position of the X-ray source is $10^h 44^m 05.09^s$, $-59° 33' 41.4''$ and has a total 1-σ error (individual source position error and systematic astrometrical uncertainty) circle radius of $\approx 0.4''$ (Broos et al. 2011). This position agrees per-

fectly (i.e. within less than $0.1''$) with the optical position of the star listed in the UCAC4 catalog ($10^h 44^m 05.091^s$, $-59° 33' 41.37''$). The positional offset to the corresponding 2MASS counterpart is $0.2''$, i.e. well within the uncertainties. From our inspection of the optical HST image we found an (insignificant) offset of $0.1''$ between the star and the X-ray source position; the nearest other star visible in the HST image is $3.8''$ offset from MJ 218. In the near-infrared HAWK-I images, we found an (insignificant) offset of $0.2''$, and a distance of $1.9''$ to the nearest other point-source. We therefore conclude that we have a clear and unambiguous identification of the X-ray source with the star MJ 218.

The X-ray properties of this source can be summarized as follows (see Broos et al. 2011, for details): the median photon energy of the source is 1.48 keV. The analysis of the photon arrival times yields some, although rather weak evidence for variability: the Kolmogorow-Smirnow test gives a probability of $P_0 = 0.16$ for the null hypothesis of a constant count rate. The fit to the X-ray spectrum with XSPEC yielded as plasma temperature of $kT = 2.5(\pm 0.8)$ keV and gave an extinction-corrected intrinsic X-ray luminosity of $L_X \approx 8.3 \times 10^{30}$ erg/sec.

According to the well established results for the origin of stellar X-ray emission (see, e.g. Güdel & Nazé 2009). no X-ray emission is expected for MJ 218, since stars of spectral type B1.5 should neither show coronal magnetic activity as typical for late-type (spectral types F and later) stars, nor should they have sufficiently strong stellar winds, in which X-ray emission is produced in wind shocks, as observed in the (much more luminous) O-type stars. The general lack of intrinsic X-ray emission from stars in the spectral type range from $\sim$ B1 to late A has been well confirmed in numerous X-ray observations (e.g., Schmitt et al. 1985; Daniel et al. 2002; Preibisch et al. 2005; Stelzer et al. 2005).

The common explanation for the detections of X-ray emission from B stars is thus the assumption that the emission actually originates from an unresolved late-type companion (e.g., Evans et al. 2011). The observed median photon energy and the plasma temperature of MJ 218 derived from the X-ray spectrum are fully consistent with this assumption, and considerably higher than one would expect from wind-shock related X-ray emission (e.g., Kudritzki & Puls 2000). Considering the general correlation between X-ray luminosity and stellar mass for young stars (see Preibisch et al. 2005), the observed X-ray luminosity suggests the companion to have a stellar mass around $\sim 1 - 2\,M_\odot$. Given the above described upper limit for a possible angular offset of the X-ray source from the B-star position of $\lesssim 0.2''$, the putative low-mass companion must have a projected separation of less than ~ 460 AU from the B-star. This rather small value makes a chance projection highly unlikely.[2] Since many B-type stars are known to have lower-mass companions at separations of a few ten to a few hundred AUs (see, e.g., Preibisch et al. 1999; Kouwenhoven et al. 2007; Grellmann et al. 2013) the hypothesis of a binary

---

[2] In order to quantify this statement, we inspected the HST image and counted the number of detectable stars within $10''$ of MJ 218 to be 8. With this estimate of the local star density, the Poisson probability to find one or more unrelated stars as chance projection within $0.2''$ of MJ 218 is just 0.3%.

system seems to be the best explanation of the observed parameters.

We searched in the HST images for such a companion, but even the narrow-band images are saturated at the required small distances from the position of MJ 218 due to the brightness of the star.[3]

3. THEORETICAL CONSIDERATIONS
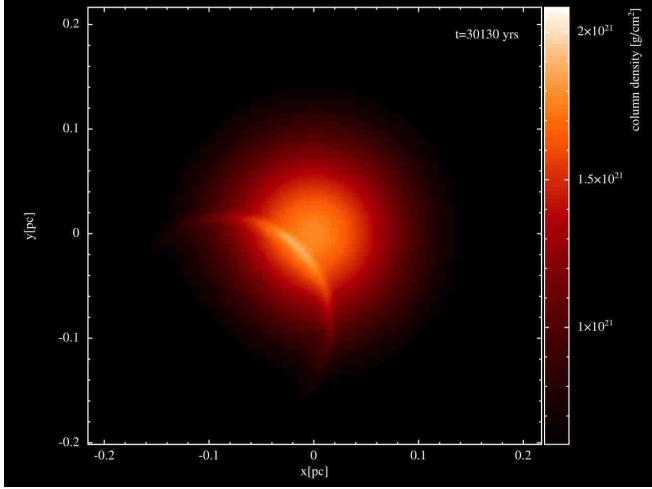
3.1. Clump carving scenario

FIG. 3.— Integrated density plot for a projected star-clump distance $d_{obs} = 0.11$ pc at an inclination of $\alpha = 66°$. The image was produced using SPLASH (Price 2007)

The evolution of the wind bubble around a star located at the edge of a clump can lead to a crescent-like shaped shock front. We performed a simulation using the Smoothed Particle Hydrodynamics (SPH) code SEREN (Hubber et al. 2011) including a newly implemented HEALPix-based (Górski et al. 2005) momentum conserving stellar wind-scheme (Ngoumou et al. 2013, in preparation) to simulate the expansion of a momentum driven wind bubble in a molecular clump. The choice of momentum driven (Steigman et al. 1975) as opposed to thermal pressure driven (Castor et al. 1975; Weaver et al. 1977) is justified, as the stellar winds of a spectral type B1.5 are assumed to be too weak to induce a hot shocked, X-ray emitting layer.

The clump was modeled as a supercritical Bonnor-Ebert sphere (Bonnor 1956; Ebert 1957), which is a self-gravitating isothermal sphere confined by an external pressure. The sphere has the dimensionless radius $\xi = 8$ and a finite radius $R_{BES} \approx 0.31$ pc, corresponding to a FWHM size of ~ 0.2 pc and a central density of $\rho_{BES} \approx 1.7 \times 10^{-19}\,\mathrm{g\,cm^{-3}}$ at a temperature of 36 K, for a total mass of $M_{clump} = 40\,M_\odot$. A static momentum source was placed at the edge of the nebula at a distance of 0.29 pc from the center of the clump. We used the mass loss rate and terminal wind velocity for a B1.5 V star as stated by Smith (2006): $\dot{M}_w = 6 \times 10^{-8}\,M_\odot\,\mathrm{yr}^{-1}$ and $v_\infty = 960\,\mathrm{km\,s}^{-1}$.

[3] The HST images (Fig. 2) show a double diffraction spike indicative of a companion separated by about 0.2 arcsec in north-south direction. The similar brightness of this potential companion, however, disqualifies it as X-ray source.

After a few 10^4 yrs, the crescent has reached the size of the observed object. To match the observed projected distance $d_{obs} \approx 0.11$ pc between the star and the center of the clump (inferred from the sub-mm map), the simulation box is rotated by an angle $\alpha = 66°$ around the axis passing the center of the clump and perpendicular to the clump-star axis. Fig. 3 shows the density integrated along the line of site at $t = 3 \times 10^4$ yrs when the crescent has reached the size of the Sickle. The inclination angle between the plane containing the star and the center of the clump, and the projection plane is $\alpha = 66°$.

This scenario though, requires the star to be embedded inside the clump. It seems unlikely that MJ 218 was born inside or close to the clump as it would certainly have been dispersed by the stellar wind by now. The assumption that the star is coming from somewhere else and travelled through the ISM, finding itself embedded inside the clump would require wind shell radii smaller than the radius of the clump. Shells with larger radii would overrun the clump, and compress it (Bisbas et al. 2011; Gritschneder et al. 2010; Tremblin et al. 2012) leading to a cometary/pillar like structure with the tail pointing away from the star. This is not observed. The required compact shell could be produced naturally if the star would move supersonically through the ISM. In this case, a star produces a bow shock with smaller radii at the collision front of the wind with the ambient medium, which we discuss in the next section.

3.2. Bow schock scenario

The reported velocity of MJ 218 is very high ($\sim 96\,\mathrm{km\,s}^{-1}$). The errors, however, are of the order of 55%, making the value rather uncertain. A star with such high velocity forms a bow shock while traveling through an ambient medium with temperatures $T \leq 10^6$ K. Indeed, the position of the tip of the arc approximately correlates with the direction of the velocity vector in the plane of the sky as inferred from proper motion measurements of the star (see Fig. 2). To test this scenario we compare the distance between the star and the cusp of the Sickle nebula with the stand-off radius R_0 inferred from the analytical solution for the shape of a stellar wind bow shock in the thin-shell limit as derived in Wilkin (1996). R_0 depends on the velocity of the star v_*, on the wind mass loss rate $\dot{M}_w$, on the terminal wind velocity v_w and on the ambient density ρ_{AMB}.

$$R_0 = \sqrt{\frac{\dot{M}_w v_w}{4\pi \rho_{AMB} v_*^2}} \qquad (1)$$

The shape of the bow shock near the stand-off radius is given by:

$$R_\theta = R_0 \operatorname{cosec}\theta \sqrt{3\left(1 - \theta \cot\theta\right)} \qquad (2)$$

with θ being the polar angle measured from axis given by the direction of motion of the star (see Fig. 4).

Fig. 5 shows the variation of the stand-off radius of the bow shock with ambient density (Eq. 1) for a range of stellar velocities and for two sets of wind parameters P1(red dot-dashed) and P2(blue dashed).

P1: $\dot{M}_w = 1.1 \times 10^{-8}\,M_\odot\,\mathrm{yr}^{-1}$; $v_\infty = 1400\,\mathrm{km\,s}^{-1}$ (based
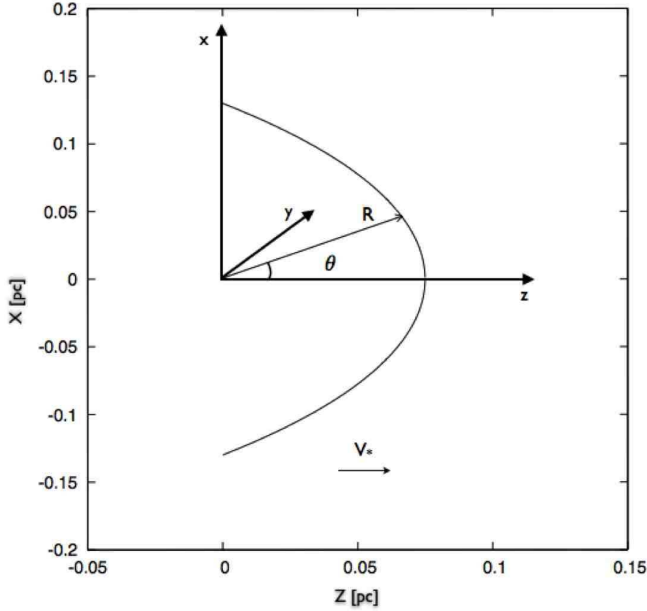
FIG. 4.— Schematic diagram of a stellar wind bow shock to illustrate the definition of the coordinate system.

on models computed by Pauldrach et al. 2001) [4]

P2: $\dot{M}_{\rm w} = 6 \times 10^{-8}\,{\rm M}_\odot\,{\rm yr}^{-1}$; $v_\infty = 960\,{\rm km\,s}^{-1}$ (Smith 2006)

The shaded area represent the spread due to the 55% error on v_*. The horizontal solid line indicates the stand-off radius inferred from the reported proper motion and radial velocity measurements which indicate an inclination angle of $\sim 6°$ and a value of R_0 of ~ 0.075 pc. The star is almost moving in the plane of the sky.

The observed stand-off distance is obtained for number densities ranging between $\sim 0.1\,{\rm cm}^{-3}$ and $\sim 20\,{\rm cm}^{-3}$. The range of ambient densities is given by the large errors on the velocity estimate for MJ 218 (shaded area in Fig. 5). For the reported $\sim 96\,{\rm km\,s}^{-1}$, $n_{AMB} = 2\,{\rm cm}^{-3}$ for P1 and $n_{AMB} = 8\,{\rm cm}^{-3}$ for P2. These values are consistent with an order-of-magnitude estimate for the density of the rather diffuse gas in the inner parts of the Carina Nebula superbubble, through which the star is moving. This hints at the Sickle being the bow shock induced by MJ 218 moving supersonically through the diffuse ISM and not directly interacting with the densest part of the clump.

The question now arises whether we just see a star with a bow shock projected in front of an unaffected clump. Interestingly, the bow shock does not appear to be symmetric around the axis given by the velocity vector of MJ 218 (see upper right panel in Fig. 2) as expected if the star would move in isolation. We therefore suggest that we indeed see a contribution from the clump. Wilkin (2000) investigated the modifications of bow shocks of stars running into an ambient density gradient in the direction perpendicular to the stellar motion and the effect of anisotropic winds. In both cases he found configurations in which the star does not lie on the symmetry axis
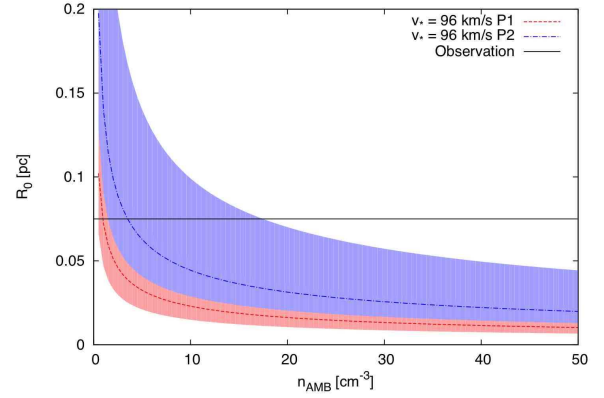
_____

[4] see http://www.usm.uni-muenchen.de/people/adi/Models/Model.html

FIG. 5.— Stand-off radius of the bow shock (Eq. 1) against number density of the ambient medium for $v_* = 96\,{\rm km\,s}^{-1}$ and for two sets of stellar wind parameters; P1 (red dot-dashed): $\dot{M}_{\rm w} = 1.1 \times 10^{-8}\,{\rm M}_\odot\,{\rm yr}^{-1}$ and $v_\infty = 1400\,{\rm km\,s}^{-1}$; P2 (blue dashed): $\dot{M}_{\rm w} = 6 \times 10^{-8}\,{\rm M}_\odot\,{\rm yr}^{-1}$ and $v_\infty = 960\,{\rm km\,s}^{-1}$. The shaded area represent the spread due to the 55% error on v_*. The horizontal solid line indicates the stand-off radius inferred from observations.

dividing the bow shock into two parts. The observed asymmetry for the position of MJ 218 with respect to the tip of the Sickle might therefore be an indication of an interaction of the moving star with the clump. As an
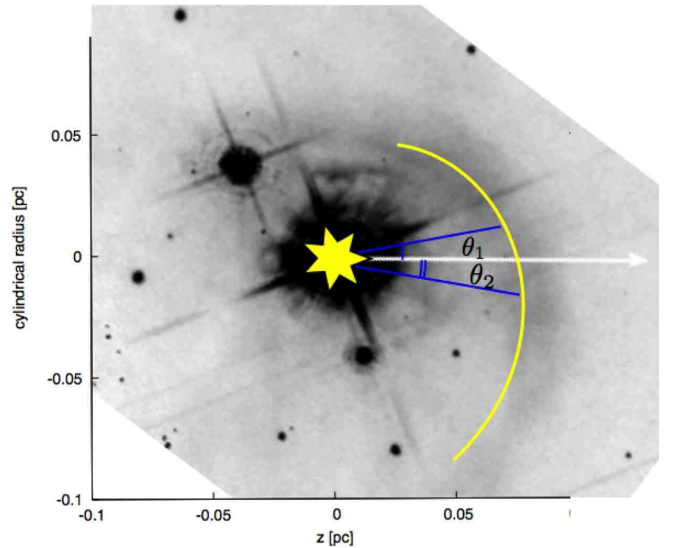

FIG. 6.— Illustration of a bow shock solution in a linear stratified medium with slope $a \approx 15\,{\rm pc}^{-1}$ for $R_0 = 0.075$ pc overlaid on an HST image (F550M band filter; image is rotated by 36°). The velocity vector points in z-direction.

illustration we consider the solution for a bow shock of a star moving in a linear stratified medium with a density gradient perpendicular to the stellar velocity vector as described in Wilkin (2000):

$$\rho_{AMB} = \rho_0 \left(1 + ay\right) \tag{3}$$

The characteristics of the solution near the stand-off point for a bow shock seen from the side (i.e. v_* perpendicular to the line-of-sight) are given by (see Eq. (71) in

Wilkin (2000)):

$$\frac{R_\theta}{R_0} = 1 - \frac{aR_0}{4}\theta + \left[\frac{1}{5} + \frac{5}{32}a^2R_0^2\right]\theta^2 \qquad (4)$$

We approximate the gradient a by selecting two points on the observed bow and measure their respective angles θ_1 and θ_2 and the corresponding distances R_{θ_1} and R_{θ_2} from the star. From Eq. 4 we estimate to first order:

$$a = \frac{4}{R_0^2}\left(\frac{R_{\theta_1} - R_{\theta_2}}{\theta_2 - \theta_1}\right) \qquad (5)$$

Fig. 6 shows the result of this approximation (yellow arc) for $R_{\theta_1} \approx 0.95R_0$ at $\theta_1 \approx 10°$ and for $R_{\theta_2} \approx 1.05R_0$ at $\theta_2 \approx -10°$. The model illustrates the non axis-symmetric shape of the bow shock induced by the additional term in the linear term near the stand-off point.

The asymmetric shape of the Sickle could be the result of MJ 218 running in a medium stratified in the direction perpendicular to its motion which coincides with the line-of-sight and the position in the sky of the clump. The observed clump could therefore be part of the stratification and be located behind the Sickle.

4. CONCLUSION

The Sickle nebulosity in the Carina Nebula is by itself already a very remarkable and interesting feature. The discovery of a dense cloud clump at a projected location just in front of the Sickle prompted us to investigate a possible relation between these two features. We simulated the impact of the momentum transfer from the stellar wind on a clump with the star being located at the edge of the clump. The off-center expansion of the wind bubble could create a crescent-like front which resembles the observed Sickle nebula. This scenario, however, requires a static source embedded in the clump. The star would have to be formed in the last $10\,000$ yrs at this position. This seems very unlikely. We therefore exclude this scenario.

Measurements of the proper motion of MJ 218 taken from the UCAC 4 catalogue (Zacharias et al. 2012) indicate a high velocity of nearly $v_* = 96\,\mathrm{km\,s^{-1}}$. At this velocity the wind of MJ 218 would form a bow shock while traveling through an ambient medium with temperatures $T \leq 10^6$ K. The Sickle could be part of the bow shock of MJ 218 seen from the side, as MJ 218 appears to be moving almost in the plane of the sky. Assuming the stand-off radius to be the distance between the star and the intersection of its velocity vector with the Sickle, we measure a stand-off radius $R_0 \approx 0.075$ pc. Such values for R_0 point at ambient densities in the range of $\sim 0.1\,\mathrm{cm^{-3}}$ and $\sim 20\,\mathrm{cm^{-3}}$ which are far lower than the $10^4\,\mathrm{cm^{-3}}$ inferred for the center of the observed clump. The star is thus not moving through the inner, central parts of the clump, but seems to be grazing along the surface of the clump.

The non-axisymmetric appearance of the Sickle is consistent with the presence of a density gradient perpendicular to the direction of motion of MJ 218, which coincides with the line-of-sight and the location of the clump. We therefore argue that the observed Sickle is part of the bow shock of the high velocity B-star MJ 218 grazing the front surface density gradient of the observed compact clump. The asymmetry of the Sickle with respect

to MJ 218 can then be explained as a result of this interaction.

We expect the Sickle to be a rather transient feature which is likely to evolve on timescales of order 10^4 yrs. Surely more detailed observation of this peculiar object will help to better constrain its nature. Spectral information from the molecular material could probe the velocity structure inside the clump and help test our star-clump interaction scenario. An interesting question is also whether the passage of the star could trigger the gravitational collapse of the clump and lead to star formation. This issue will be addressed in a subsequent paper. In addition a closer look at the binary nature of MJ 218 and its implications could help shed a light on the complex history of the Carina Nebula. Especially the question of the origin MJ 218 in the framework of the formation of massive runaway binaries (McSwain et al. 2007; Gvaramadze et al. 2011, 2012) would be worth investigating. The direction of the velocity vector of MJ 218 suggests a possible origin in the open cluster Trumpler 16 in the center of the Carina Nebula. The observed proper motion would then imply a travel time of about 10^5 yrs. It is very interesting to note that the back-projected motion path puts MJ 218 in close vicinity of a recently detected neutron star candidate in the Carina Nebula, described in Hamaguchi et al. (2009). This raises the possibility that MJ 218 has perhaps been ejected in a relatively recent supernova explosion in the Carina Nebula. Further investigations of this relations could thus provide interesting information on the dynamical evolution, stellar clustering (Moeckel & Bate 2010) and the still very unclear history of past supernovae in the Carina Nebula.

REFERENCES

Ascenso, J., Alves, J., Vicente, S., & Lago, M. T. V. T. 2007, A&A , 476, 199

Bisbas, T. G., Wünsch, R., Whitworth, A. P., Hubber, D. A., & Walch, S. 2011, ApJ , 736, 142

Blaauw, A. 1961, Bull. Astron. Inst. Netherlands, 15, 265

Bonnor, W. B. 1956, MNRAS , 116, 351

Broos, P. S., Townsley, L. K., Feigelson, E. D., et al. 2011, ApJS, 194, 2

Castor, J., McCray, R., & Weaver, R. 1975, ApJ, 200, L107

Dale, J. E., & Bonnell, I. 2011, MNRAS , 414, 321

Daniel, K. J., Linsky, J. L., & Gagné, M. 2002, ApJ , 578, 486

Deharveng, L., Schuller, F., Anderson, L. D., et al. 2010, A&A , 523, A6

Ebert, R. 1957, ZAp, 42, 263

Evans, N. R., DeGioia-Eastwood, K., Gagné, M., et al. 2011, ApJS, 194, 13

Fierlinger, K. M., Burkert, A., Diehl, R., et al. 2012, Advances in Computational Astrophysics: Methods, Tools, and Outcome, 453, 25

Górski, K. M., Hivon, E., Banday, A. J., et al. 2005, ApJ , 622, 759

Grellmann, R., Preibisch, T., Ratzka, T., et al. 2013, A&A , 550, A82

Griffin, M. J., Abergel, A., Abreu, A., et al. 2010, A&A , 518, L3

Gritschneder, M., Burkert, A., Naab, T., & Walch, S. 2010, ApJ , 723, 971

Güdel, M., & Nazé, Y. 2009, A&A Rev., 17, 309

Gvaramadze, V. V., Röser, S., Scholz, R.-D., & Schilbach, E. 2011, A&A , 529, A14

Gvaramadze, V. V., Weidner, C., Kroupa, P., & Pflamm-Altenburg, J. 2012, MNRAS , 424, 3037

Hamaguchi, K., Corcoran, M. F., Ezoe, Y., et al. 2009, ApJ, 695, L4

Huang, W., & Gies, D. R. 2006, ApJ , 648, 580

Hubber, D. A., Batty, C. P., McLeod, A., & Whitworth, A. P. 2011, A&A , 529, A27

Kobulnicky, H. A., & Fryer, C. L. 2007, ApJ , 670, 747

Kobulnicky, H. A., Lundquist, M. J., Bhattacharjee, A., & Kerton, C. R. 2012, AJ, 143, 71

Kouwenhoven, M. B. N., Brown, A. G. A., Portegies Zwart, S. F., & Kaper, L. 2007, A&A , 474, 77

Kudritzki, R.-P., & Puls, J. 2000, ARA&A, 38, 613

Lada, C. J., & Lada, E. A. 2003, ARA&A, 41, 57

Mason, B. D., Gies, D. R., Hartkopf, W. I., et al. 1998, AJ, 115, 821

Massey, P., & Johnson, J. 1993, AJ, 105, 980

McSwain, M. V., Ransom, S. M., Boyajian, T. S., Grundstrom, E. D., & Roberts, M. S. E. 2007, ApJ , 660, 740

Moeckel, N., & Bate, M. R. 2010, MNRAS , 404, 721

Mottram, J. C., Hoare, M. G., Lumsden, S. L., et al. 2007, A&A , 476, 1019

Ntormousi, E., Burkert, A., Fierlinger, K., & Heitsch, F. 2011, ApJ , 731, 13

Oey, M. S., & García-Segura, G. 2004, ApJ , 613, 302

Ohlendorf, H., Preibisch, T., Gaczkowski, B., et al. 2012, A&A , 540, A81

Pauldrach, A. W. A., Hoffmann, T. L., & Lennon, M. 2001, A&A , 375, 161

Poglitsch, A., Waelkens, C., Geis, N., et al. 2010, A&A , 518, L2

Preibisch, T., Roccatagliata, V., Gaczkowski, B., & Ratzka, T. 2012, A&A , 541, A132

Preibisch, T., Ratzka, T., Kuderna, B., et al. 2011d, A&A , 530, A34

Preibisch, T., Ratzka, T., Gehring, T., et al. 2011c, A&A , 530, A40

Preibisch, T., Hodgkin, S., Irwin, M., et al. 2011b, ApJS, 194, 10

Preibisch, T., Schuller, F., Ohlendorf, H., et al. 2011a, A&A , 525, A92

Preibisch, T., Kim, Y.-C., Favata, F., et al. 2005, ApJS, 160, 401

Preibisch, T., Weigelt, G., & Zinnecker, H. 2001, The Formation of Binary Stars, 200, 69

Preibisch, T., Balega, Y., Hofmann, K.-H., Weigelt, G., & Zinnecker, H. 1999, New Astronomy, 4, 531

Price, D. J. 2007, Publ. Astron. Soc. Aust., 24, 159

Reed, B. C. 2003, AJ, 125, 2531

Schmitt, J. H. M. M., Golub, L., Harnden, F. R., Jr., et al. 1985, ApJ , 290, 307

Smith, N., Bally, J., & Morse, J. A. 2003, ApJ, 587, L105

Smith, N., Barbá, R. H., & Walborn, N. R. 2004, MNRAS , 351, 1457

Smith, N. 2006, MNRAS , 367, 763

Smith, N., & Brooks, K. J. 2007, MNRAS , 379, 1279

Smith, N., Povich, M. S., Whitney, B. A., et al. 2010, MNRAS , 406, 952

Steigman, G., Strittmatter, P. A., & Williams, R. E. 1975, ApJ , 198, 575

Stelzer, B., Flaccomio, E., Montmerle, T., et al. 2005, ApJS, 160, 557

Tapia, M., Roth, M., Bohigas, J., & Persi, P. 2011, MNRAS , 416, 2163

Townsley, L. K., Broos, P. S., Corcoran, M. F., et al. 2011, ApJS, 194, 1

Tremblin, P., Audit, E., Minier, V., Schmidt, W., & Schneider, N. 2012, A&A , 546, A33

Urquhart, J. S., Busfield, A. L., Hoare, M. G., et al. 2007, A&A , 461, 11

Walch, S. K., Whitworth, A. P., Bisbas, T., Wünsch, R., & Hubber, D. 2012, MNRAS , 427, 625

Weaver, R., McCray, R., Castor, J., Shapiro, P., & Moore, R. 1977, ApJ , 218, 377

Wilkin, F. P. 1996, ApJ, 459, L31

Wilkin, F. P. 2000, ApJ , 532, 400

Wilson, T. L., Rohlfs, K., Hüttemeister, S. 2009, Tools of Radio Astronomy, by Thomas L. Wilson; Kristen Rohlfs and Susanne Hüttemeister. ISBN 978-3-540-85121-9. Published by Springer-Verlag, Berlin, Germany, 2009

Zacharias, N., Finch, C. T., Girard, T. M., et al. 2012, VizieR Online Data Catalog, 1322, 0

Zacharias, N., Finch, C. T., Girard, T. M., et al. 2013, AJ, 145, 44